aan5353

Title:

Second messenger-mediated tactile response by a bacterial rotary motor

Authors:

Isabelle Hug[1], Siddharth Deshpande[2,3], Kathrin S. Sprecher[1], Thomas Pfohl[2,4], Urs Jenal[1*]

Affiliations:

[1] Biozentrum, University of Basel, Klingelbergstrasse 50/70, CH-4056, Switzerland.

[2] Department of Chemistry, University of Basel, Klingelbergstrasse 80, CH-4056, Switzerland.

Current addresses:

[3] Department of Bionanoscience, Delft University of Technology, Van der Maasweg 9, 2629 HZ Delft, The Netherlands.

[4] Institute of Physics, University of Freiburg, Hermann-Herder-Str. 3, 79104 Freiburg, Germany

*Correspondence to: urs.jenal@unibas.ch.

1   **Abstract**

2   When bacteria encounter surfaces, they respond by surface colonization and virulence induction. The

3   mechanisms of bacterial mechanosensation and downstream signaling remain poorly understood.

4   Here, we describe a tactile sensing cascade in *Caulobacter crescentus*, in which the flagellar motor

5   acts as sensor. Surface-induced motor interference stimulated the production of the second messenger

6   c-di-GMP by the motor-associated diguanylate cyclase DgcB. This led to the allosteric activation of

7   the glycosyltransferase HfsJ to promote rapid synthesis of a polysaccharide adhesin and surface an-

8   choring. While the membrane embedded motor unit was essential for surface sensing, mutants lack-

9   ing external flagellar structures were hypersensitive to mechanical stimuli. Thus, the bacterial flagel-

10   lar motor acts as a tetherless sensor reminiscent of mechanosensitive channels.

11

12

13

14   **One Sentence Summary**

15   Surface sensing by a flagellar rotary motor induces rapid attachment via c-di-GMP mediated produc-

16   tion of an exopolysaccharide adhesin.

17
18

19   Mechanical cues are perceived by bacteria during surface contact, leading to a rapid change in

20   behavior by inducing adherence and biofilm formation, surface motility or virulence (*1-3*). Structures

21   involved in bacterial surface interaction include pili and flagella. Models for bacterial mechanosensa-

22   tion proposed that pili transiently establish surface contact, eliminating the space required for free ro-

23   tation of the flagellum and increasing the load on the motor (*1, 4-6*). As a consequence, intracellular

24   sensory proteins could detect conformational rearrangements of motor proteins or an altered proton

25   flux through the motor (*7, 8*). However, these models remain controversial and recent studies have

26   challenged the role of the flagellum as a key player in surface detection (*9, 10*). We hypothesized that

27   some of these inconsistencies could be attributed to analyzing surface colonization at different time-

28   scales, a problem that can be avoided by rigorously separating the individual stages of surface coloni-

29   zation through careful experimental design. We chose the surface-stimulated synthesis of the adhe-

30   sive holdfast of *Caulobacter crescentus* to dissect bacterial mechanosensation. Newborn *C. crescen-*

31   *tus* swarmer (SW) cells are equipped with a single flagellum (Fig. 1A) and are motile for a defined

32   period before shedding their flagellum and secreting the holdfast, a polysaccharide adhesin that per-

33   manently anchors cells to the surface. However, when SW cells encounter a solid substratum they de-

34   ploy a holdfast within seconds, a process that can be imaged in real time using fluorescently labeled

35   holdfast-specific lectins (*6, 11*).

36   To experimentally assess surface-stimulated holdfast formation, we employed a set of microflu-

37   idics-based techniques that impose close surface contact on *C. crescentus* (Fig. 1B,C) (*12*). Offspring

38   of attached mothers are exposed to surface as a consequence of medium flow over the crescentoid

39   dividing cells, which positions the flagellated and piliated pole in close proximity to the substratum

40   (*9*) (Fig. 1B). Under these conditions, about 50% of the daughters remained attached directly down-

41   stream of their mothers and often displayed a holdfast before separating (Figs. 1B,D,E; S1A-D;

42   Movie S1). Thus, future SW cells acquired the ability to respond to surface exposure before separa-

43   tion. At this stage, the flagellum is fully assembled and actively rotating (Movie S2). High speed im-

44   aging of cells dividing under flow revealed that SW offspring rotating around their long axis before

45   separation were generally washed away, while SW cells that managed to adhere, remained static or

46   stopped their rotation before budding off (Fig. S1E; Movies S2-S4). These observations are in agree-

47   ment with pili-mediated immobilization of the cell body and flagellar obstruction being vital for SW

48   cells to sense surface. Consistent with this, polar pili were strictly required for rapid attachment (Fig.

49   1E). When grown under flow, a single mother generated small microcolonies through cycles of divi-

50   sion and attachment of SW offspring (Fig. 1F, Movie S5). The area covered by such colonies was

51   proportional to the attachment efficiency of SW progeny (Fig. 1E,G). Surprisingly, SW cells of mu-

52   tants lacking outer parts of the flagellum, including proximal and distal rods (Δ*flgFG*), hook and fila-

53   ment (Δ*flgDE*) (Fig. 1A), showed higher propensity to attach than the wild type (Fig. 1E,G), arguing

54   against the flagellum acting as a simple tactile tether. This was not due to an altered developmental

55   timing of holdfast formation but rather to a hypersensitive tactile response (Fig. S2). In contrast, mu-

56   tants that failed to assemble the inner parts of the motor (Δ*fliFG*) as well as mutants with a fully as-

57   sembled but paralyzed flagellum (Δ*motA*, Δ*fliL*, Δ*motB*, $motB_{D33N}$) failed to attach effectively (Fig.

58   1E,G). Alleles compromising internal motor components or the pilus were dominant over alleles af-

59   fecting external flagellar parts (Fig. 1G), demonstrating that cells lacking hook and filament but with

60   an intact internal motor remained fully responsive to surface. Thus, the integrity and activity of the

61   motor but not the external parts of the rotary flagellum are required for surface sensing.

62   To corroborate these findings and to address the role of the pili in surface signaling, we de-

63   signed thin, diffusion-controlled quasi-2D chambers (*12*) to follow SW progeny microscopically

64   from the moment of birth at division to the onset of holdfast production (Fig. 1C). With a height of

65   only 0.75 μm such micro-chambers offer cells constant surface interaction opportunities without me-

66   dium flow. Accordingly, we observed the formation of holdfast within a few seconds after newborn

67   SW cells were released from their mothers (Fig. 1H). The tight geometry of these chambers allevi-

68   ated the strict requirement of adhesive pili (Δ*pilA*) and putative pili motor components (Δ*cpaE*,

69   Δ*cpaF*) for surface recognition (Fig. 1H). In contrast, a paralyzed mutant with a MotB stator subunit

70   unable to conduct protons (MotB$_{D33N}$) (*13*, *14*) but harboring unaltered pili developed holdfast only

71   about 10 minutes after division, corresponding roughly to the time required for the completion of the

72   developmental program leading to holdfast formation (Fig. 1H). Thus, rather than playing a direct

73   role as surface sensors, the function of pili is to bring the cell pole into close proximity with the un-

74   derlying surface to facilitate effective sensing by the motor.

75   The machinery for holdfast biosynthesis is on standby in dividing and newborn SW cells, wait-

76   ing for an activating trigger (*15*, *16*). This, and the observed speed of holdfast production argued that

77   the tactile response is regulated posttranslationally. A prime candidate to fulfill this function is the

78   second messenger c-di-GMP, which promotes surface adaptation in many bacteria (*17*) and controls

79   holdfast production during *C. crescentus* development (*18*, *19*). To investigate the role of c-di-GMP

80   in the *C. crescentus* surface response, we used a strain in which the c-di-GMP concentration can be

81   experimentally tuned. In this strain all genes encoding endogenous diguanylate cyclases and phos-

82   phodiesterases were deleted and substituted with the P$_{lac}$-driven *dgcZ* diguanylate cyclase gene form

83   *Escherichia coli* (rcdG^0 P$_{lac}$::*dgcZ*). While the rcdG^0 strain itself is unable to assemble pili and hold-

84   fast and thus fails to adhere to surfaces, moderate induction of *dgcZ* restored organelle assembly (*18*)

85   and enabled the formation of microcolonies under flow conditions (Fig. 2). Constitutive synthesis of

86   c-di-GMP bypassed the requirement of an active motor for rapid attachment (Fig. 2), while pili re-

87   mained important for attachment (Fig. 2) but were also not required for holdfast biogenesis (Fig. S3).

88   Thus, c-di-GMP acts downstream of the motor to induce a rapid surface response. When analyzing *C.*

89   *crescentus* mutants lacking individual diguanylate cyclases, only deletion of *dgcB* strongly reduced

90   attachment of newborn SW cells, a defect that could be complemented by adding *dgcB in trans* (Figs.

91   2, S4). Likewise, a point mutation abolishing DgcB catalytic activity (E261Q) eliminated rapid sur-

92   face attachment (Fig. 2). Together with the observation that DgcB does not contribute to the c-di-

93   GMP pool in liquid cultures (*18*), these data inferred a specific role for DgcB in *C. crescentus* surface

94   sensing.

95   DgcB localized to the flagellated pole (*20*) in 16.1 % of dividing and in 30.6 % of SW cells

96   (n=242 and 292, respectively) (Fig. S5A, Movie S6). Although polar localization of DgcB did not

97   depend on the presence of components of the flagellar motor (Fig. S5A), pulldown experiments re-

98   vealed MotA in the elution fraction of tagged DgcB. Inversely, DgcB was pulled down when tagged

99   MotA served as bait (Fig. S5B). This argued that DgcB is located in close proximity of the stator

100   units and that spatial coupling may facilitate signal transduction. DgcB has a C-terminal catalytic

101   GGDEF domain and an N-terminal domain of unknown function. DgcB homologs with an ortholo-

102   gous N-terminal domain are widespread in bacteria including *Vibrio* or *Pseudomonas* species (Fig.

103   S6A,B). A motif search with amino acids conserved in the N-terminal domain of DgcB (Fig. S6C)

104   identified diguanylate cyclases, oxidoreductases and inner membrane transporters (Table S1), sug-

105   gesting that these domains might tap into the redox/energy status at the inner membrane. Mutating

106   highly conserved residues of this motif (N35A, F36A, W39A) strongly reduced *C. crescentus* surface

107   induced attachment (Fig. S6D) without affecting DgcB protein stability (Fig. S6E). This is in line

108   with the idea that the N-terminus serves as an input domain to regulate DgcB activity. Thus, *Cau-*

109   *lobacter* senses mechanical cues via its polar flagellar motor, which in turn emits a physical or chem-

110   ical signal that is converted by DgcB into a pulse of c-di-GMP.

111   To identify the molecular target of c-di-GMP that is responsible for rapid holdfast production,

112   we used Capture Compound Mass Spectrometry (CCMS) (*21*). One of the proteins that was specifi-

113   cally pulled down was HfsJ, a glycosyltransferase essential for holdfast biogenesis (*22*). Biochemical

114   analyses confirmed that HfsJ bound c-di-GMP directly and specifically (Fig. 3A). HfsJ harbors an

115   arginine-rich N-terminal region, which is only conserved in homologs of close relatives of *C. cres-*

116   *centus* (Fig. 3B). This region features a triple repeat of the RXXXR motif also found in other c-di-

117   GMP effectors (*23*). Replacing R23 or R27 abolished c-di-GMP binding without affecting protein

118   stability (Figs. 3C, S7A) and strongly reduced holdfast production, akin to an HfsJ catalytic mutant

119   (R247Q) (Fig. 3D). Overexpression of *hfsJ* augmented holdfast formation in *C. crescentus* wild type

120   and restored holdfast formation in the cdG^0 strain (Fig. S7B), arguing that HfsJ activity constitutes

121   the rate limiting step in holdfast biosynthesis. Likewise, HfsJ variants unable to bind c-di-GMP, but

122   not an HfsJ catalytic mutant, restored holdfast biogenesis in the cdG^0 strain when overexpressed (Fig.

123   S7C). Thus, these mutations affected the regulation of HfsJ but not its catalytic activity per se. HfsJ is

124   also targeted by a small protein inhibitor, HfiA, which controls holdfast formation in response to nu-

125   tritional cues (*22*). Rapid attachment of a *ΔhfiA* mutant retained its strict dependency on DgcB and on

126   a functional motor, excluding a role for HfiA in mechanosensation (Fig. S7D). Thus, HfsJ is a critical

127   bottleneck in holdfast biogenesis and its activity is stimulated by c-di-GMP to rapidly boost holdfast

128   expression when DgcB is activated by tactile sensing or when c-di-GMP levels rise during SW cell

129   development.

130   Our results have uncovered an important role for the *C. crescentus* flagellar motor as a tactile

131   sensor. A simple model for sensing by surface-mediated obstruction of flagellar rotation (*1*, *4-6*) is

132   not supported by our data. Rather, the strict need for an intact motor argues that flagellar Mot pro-

133 teins may act as mechanosensitive channels. Similar to bacterial osmoregulators MscL/S (*24*) or Pi-

134 ezo2 channels in mammalian epidermal Merkel cells (*25*, *26*), surface exposure of *C. crescentus* may

135 be communicated to the cytosol via a change in ion flux through the stators, inflicted by conforma-

136 tional changes when mechanical forces impact the cell envelope. This could result in a transient pH

137 change inside the cells, which is then picked up and amplified by enzymes like DgcB (Fig. 3E). Such

138 a model conforms well with the strong pH-dependent stimulation of DgcB activity in vitro (*20*) and

139 with the observation that the $MotB_{D33N}$ mutant, which is unable to conduct protons, failed to respond

140 to surfaces similar to strains lacking components of the rotor.

References and Notes:

1. G. A. O'Toole, G. C. L. Wong, Sensational biofilms: surface sensing in bacteria. *Current Opinion in Microbiology*. **30**, 139–146 (2016).

2. A. Siryaporn, S. L. Kuchma, G. A. O'Toole, Z. Gitai, Surface attachment induces Pseudomonas aeruginosavirulence. *Proceedings of the National Academy of Sciences*. **111**, 16860–16865 (2014).

3. A. Persat *et al*., The mechanical world of bacteria. *Cell*. **161**, 988–997 (2015).

4. L. McCarter, M. Hilmen, M. Silverman, Flagellar dynamometer controls swarmer cell differentiation of V. parahaemolyticus. *Cell*. **54**, 345–351 (1988).

5. E. Karatan, P. Watnick, Signals, regulatory networks, and materials that build and break bacterial biofilms. *Microbiology and molecular biology reviews : MMBR*. **73**, 310–347 (2009).

6. G. Li *et al*., Surface contact stimulates the just-in-time deployment of bacterial adhesins. *Molecular Microbiology*. **83**, 41–51 (2012).

7. P. P. Lele, B. G. Hosu, H. C. Berg, Dynamics of mechanosensing in the bacterial flagellar motor. *Proceedings of the National Academy of Sciences*. **110**, 11839–11844 (2013).

8. K. L. Van Dellen, L. Houot, P. I. Watnick, Genetic analysis of Vibrio cholerae monolayer formation reveals a key role for DeltaPsi in the transition to permanent attachment. *Journal of Bacteriology*. **190**, 8185–8196 (2008).

9. A. Persat, H. A. Stone, Z. Gitai, The curved shape of Caulobacter crescentus enhances surface colonization in flow. *Nature Communications*. **5**, 3824 (2014).

10. A. Persat, Y. F. Inclán, J. N. Engel, H. A. Stone, Z. Gitai, Type IV pili mechanochemically regulate virulence factors in Pseudomonas aeruginosa. *Proceedings of the National Academy of Sciences*. **112**, 7563–7568 (2015).

11. M. D. Hoffman *et al*., Timescales and Frequencies of Reversible and Irreversible Adhesion Events of Single Bacterial Cells. *Analytical Chemistry*. **87**, 12032–12039 (2015).

12. S. Deshpande, T. Pfohl, Hierarchical self-assembly of actin in micro-confinements using microfluidics. *Biomicrofluidics*. **6**, 34120 (2012).

13. J. Zhou *et al*., Function of protonatable residues in the flagellar motor of Escherichia coli: a critical role for Asp 32 of MotB. *Journal of Bacteriology*. **180**, 2729–2735 (1998).

14. S. Kojima, D. F. Blair, Conformational change in the stator of the bacterial flagellar motor. *Biochemistry*. **40**, 13041–13050 (2001).

15. A. Levi, U. Jenal, Holdfast Formation in Motile Swarmer Cells Optimizes Surface Attachment during Caulobacter crescentus Development. *Journal of Bacteriology*. **188**, 5315–5318 (2006).

16. G. G. Hardy *et al*., A localized multimeric anchor attaches the Caulobacter holdfast to the cell pole. *Molecular Microbiology*. **76**, 409–427 (2010).

17. U. Jenal, A. Reinders, C. Lori, Cyclic di-GMP: second messenger extraordinaire. *Nature reviews. Microbiology*. **15**, 271–284 (2017).

18. S. Abel *et al*., Bi-modal Distribution of the Second Messenger c-di-GMP Controls Cell Fate and Asymmetry during the Caulobacter Cell Cycle. *PLoS Genetics*. **9**, e1003744 (2013).

19. K. S. Sprecher *et al*., Cohesive Properties of the Caulobacter crescentus Holdfast Adhesin Are Regulated by a Novel c-di-GMP Effector Protein. *mBio*. **8**, e00294–17 (2017).

20. S. Abel *et al*., Regulatory Cohesion of Cell Cycle and Cell Differentiation through Interlinked Phosphorylation and Second Messenger Networks. *Molecular Cell*. **43**, 550–560 (2011).

21. J. Nesper, A. Reinders, T. Glatter, A. Schmidt, U. Jenal, A novel capture compound for the identification and analysis of cyclic di-GMP binding proteins. *Journal of proteomics*. **75**, 4874–4878 (2012).

22. A. Fiebig *et al*., A cell cycle and nutritional checkpoint controlling bacterial surface adhesion. *PLoS Genetics*. **10**, e1004101 (2014).

23. S.-H. Chou, M. Y. Galperin, Diversity of Cyclic Di-GMP-Binding Proteins and Mechanisms. *Journal of Bacteriology*. **198**, 32–46 (2016).

24. I. R. Booth, S. Miller, A. Müller, L. Lehtovirta-Morley, The evolution of bacterial mechano-sensitive channels. *Cell Calcium*. **57**, 140–150 (2015).

25. R. Ikeda *et al*., Merkel cells transduce and encode tactile stimuli to drive Aβ-afferent impulses. *Cell*. **157**, 664–675 (2014).

26. S.-H. Woo *et al*., Piezo2 is required for Merkel-cell mechanotransduction. *Nature*. **509**, 622–626 (2014).

27. J. M. Schrader, L. Shapiro, Synchronization of Caulobacter crescentus for investigation of the bacterial cell cycle. *J Vis Exp*. **98**, 1–6 (2015).

28. M. Christen, B. Christen, M. Folcher, A. Schauerte, U. Jenal, Identification and Characterization of a Cyclic di-GMP-specific Phosphodiesterase and Its Allosteric Control by GTP. *Journal of Biological Chemistry*. **280**, 30829–30837 (2005).

29. H. Bruus, Bruus: *Theoretical microfluidics*. 2008 - New York: Oxford University Press.

30. K. R. Ryan, E. M. Judd, L. Shapiro, The CtrA response regulator essential for Caulobacter crescentus cell-cycle progression requires a bipartite degradation signal for temporally controlled proteolysis. *Journal of Molecular Biology*. **324**, 443–455 (2002).

31. G. Li, L.-K. Tam, J. X. Tang, Amplified effect of Brownian motion in bacterial near-surface swimming. P*roceedings of the National Academy of Sciences of the United States of America*. **105**, 18355–18359 (2008).

222   **Fig. 1**. **The flagellar motor is a tactile mechanosensor.** (**A**) Schematic representation of the bacte-

223   rial flagellum. (**B**) Progeny of mother cells attached to the glass surface in a microfluidic channel

224   were either carried away after release or expressed a holdfast (red) before separating to remain at-

225   tached downstream of the mother cell. Medium flow and chamber dimensions are indicated by blue

226   and black arrows, respectively. (**C**) Newborn cells were observed in microchambers of 0.75 μm

227   height with fluorescent WGA lectin added to the medium to determine the timespan between daugh-

228   ter cell release and the appearance of the holdfast (red). (**D**) *C. cr*escentus cell dividing in a flow

229   channel. Newly formed holdfast at the flagellated pole of a dividing cell (arrows) and time relative to

230   cell division are indicated. White scale bars are 2 μm. (**E**) Efficiency of SW cell attachment under

231   constant flow. Data are based on 232 (wt), 160 (*ΔpilA*), 88 (*ΔfliFG*), 139 (*ΔflgDE*), 88 (*ΔmotA*) and

232   107 (*ΔfliL*) individual separation events. (**F**) Microcolonies formed from growth and attachment of

233   single ancestors (arrows) in the flow channel. The area covered by the colony (yellow line) served as

234   a measure for the efficiency of rapid holdfast expression. (**G**) Areas of microcolonies after 15 h

235   growth in a flow channel illustrate the efficiency of daughter cell attachment. Box plots show median

236   (horizontal black lines), lower and upper quartiles (dark and light orange boxes) and extreme values

237   (whiskers). Values were normalized to the median of the wild type colony area. (**H**) Time between

238   release of SW progeny from their mothers to detection of holdfast. The strains were grown as illus-

239   trated in (**C**). Because motile daughters are difficult to reliably track in this assay due to their swim-

240   ming speed, only non-motile mutants were used for this analysis. Averages are shown as black lines.

241   Measurements for *ΔflgDE ΔpilA* are significantly different from measurements for *ΔflgDE motB*$_{D33N}$

242   (students T-test: $P < 0.001$).

243

244 **Fig. 2. The diguanylate cyclase DgcB is essential for surface sensing and rapid attachment.** At-

245 tachment of the strains indicated was scored as outlined in Fig. 1G. The *C. crescentus* rcdG^0

246 P$_{lac}$::*dgcZ* strain lacks all diguanylate cyclases and phosphodiesterases but carries a plasmid-born

247 copy of the P$_{lac}$-driven *dgcZ* gene from *E. coli*. In the rcdG^0::*dgcB*::*pleD* p*pdeH* strain, two diguanyl-

248 ate cyclase genes, *dgcB* and *pleD*, are retained. In addition, the strain carries a plasmid-born copy of

249 the *E. coli pdeH* gene, encoding a phosphodiesterase. The *dgcBE261A* allele carries a point mutation

250 in the active site, rendering its product catalytically inactive. Box plots show the median (horizontal

251 black lines), the lower and upper quartiles (dark and light orange boxes) and the extreme values

252 (whiskers). Values were normalized to the median of the wild type colony area.

253

254 **Fig. 3. C-di-GMP binding to HfsJ initiates holdfast biosynthesis.** (**A**) Binding of c-di-GMP to

255 HfsJ (closed circles) was measured with increasing concentrations of radiolabeled ligand as indi-

256 cated, revealing a *Kd* of 2.7 µM. Binding is specific for c-di-GMP (inlet). Radiolabeled c-di-GMP (5

257 µM) was competed with a 100x excess of the nucleotides indicated and overall binding was deter-

258 mined. (**B**) Alignment of the N-termini of HfsJ orthologs from *C. crescentus* (*C.c.*) and the following

259 closely related species: *C. henricii* (*C.h.*), *Caulobacter* sp. K31 *(C.sp.)*, *Brevundimonas diminuta*

260 *(B.d.)*, *B. naejangsanensis (B.n.)*, *A. biprosthecium (A.b.)*, *A. benevestitus (A.b.)*, *Deinococcus*

261 *apachensis (D.a.)*, *Rhodothermus marinus (R.m.)*, *Lihuaxuella thermophile (L.t.)*. Conserved residues

262 are highlighted with arginines in red, negative charges in green and proline or aromatic amino acids

263 in blue. (**C**) Binding studies with HfsJ identified R23 and R27 as critical residues for c-di-GMP bind-

264 ing. The highly-conserved catalytic residue R247 is not required for c-di-GMP binding. (**D**) In vivo

265 activity of HfsJ. Cells of *C. crescentus* wild type (n=764) and *hfsJ* mutants (R23Q, n=1077; R247Q,

266 n=6) were grown in the presence of Oregon Green 488-labelled WGA lectin and holdfast biogenesis

267 was measured as relative fluorescence intensities of individual cells. (**E**) Model of *C. crescentus* sur-

268 face sensing. Initial surface adherence is mediated by pili and pili retraction positioning the flagellar

269 pole in close contact with the surface. The physical pressure applied on the cell envelope by the sur-

270 face impacts the function of the flagellar rotor-stator components, generating an unknown signal that

271 is sensed by DgcB and is converted into a burst of c-di-GMP (red). The second messenger initiates

272 rapid holdfast biogenesis and permanent attachment by activating the key glycosyltransferase HfsJ.

273

274

275

276 **Supplementary Materials:**

277 Materials and Methods

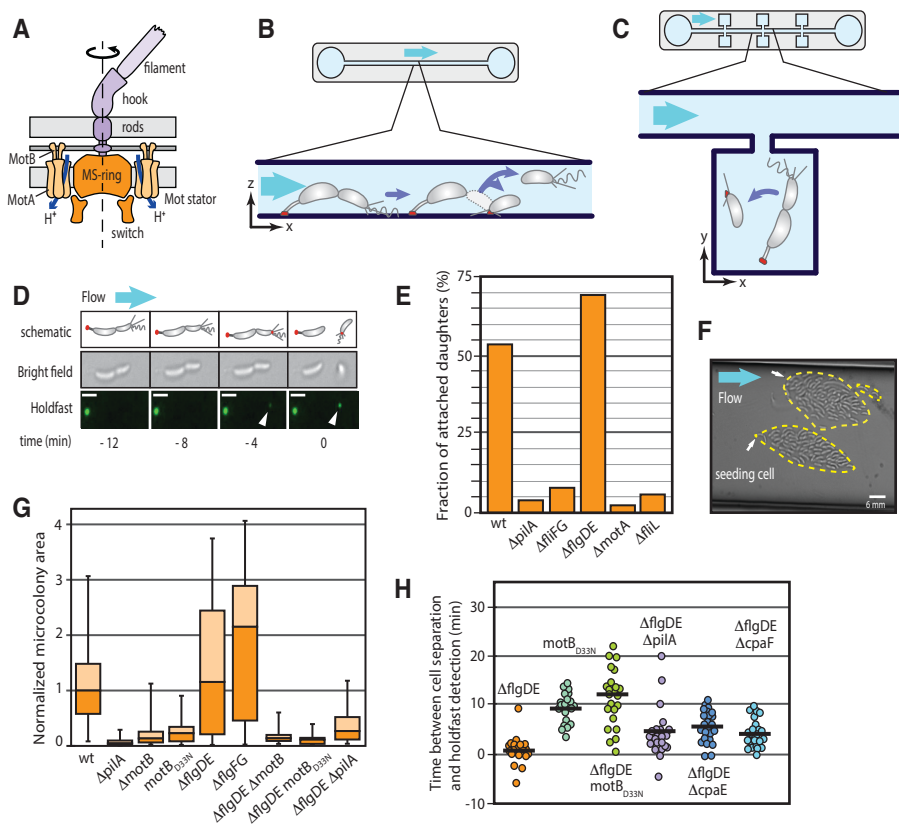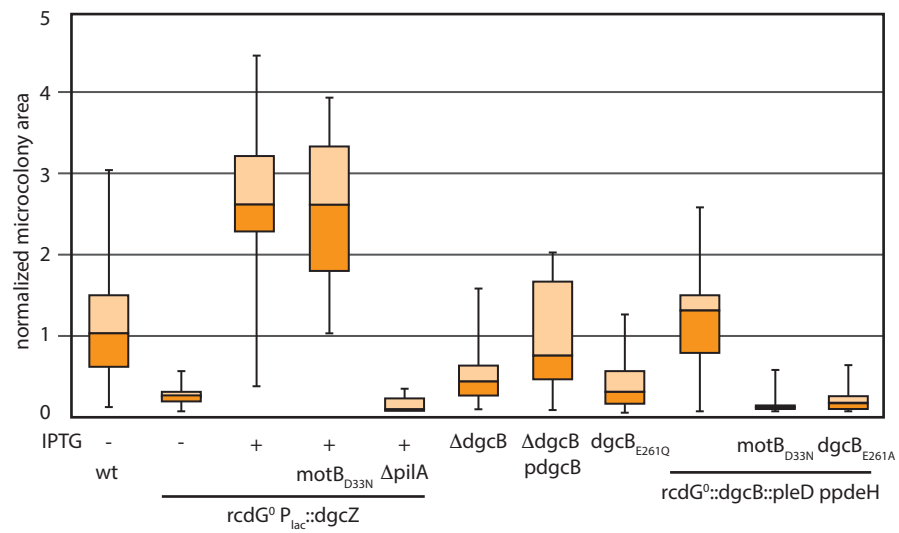278 Figures S1-S7

279 Tables S1-S4

280 Movies S1-S6
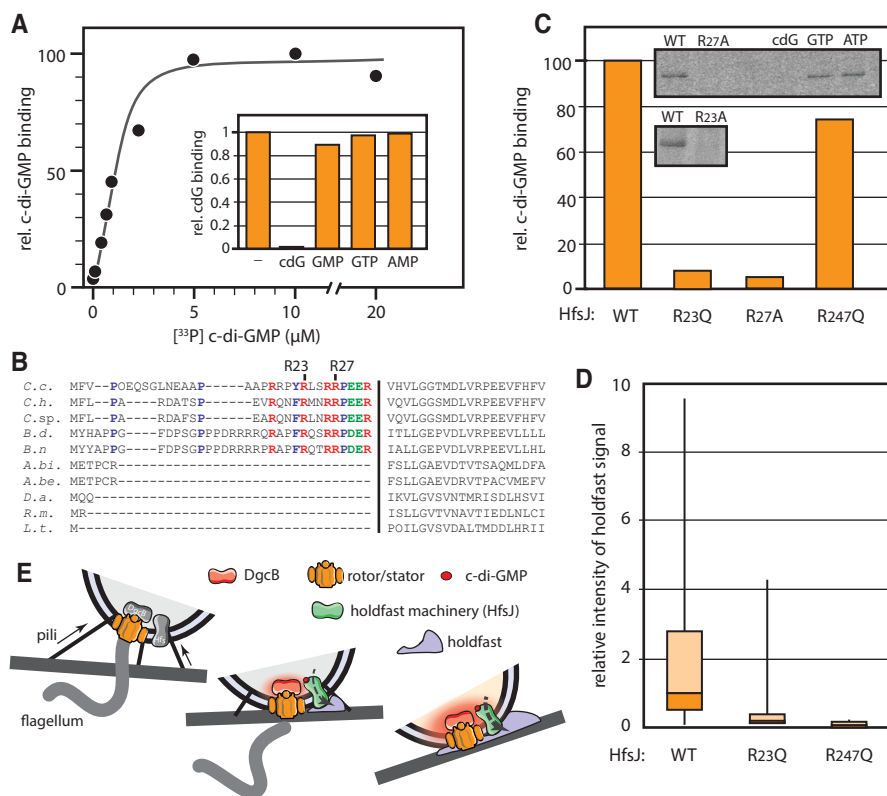
281 References (*27-31*)

282

283 **Author contributions**

284 I.H., S.D., T.P. and U.J. designed the study; I.H., S.D. and K.S.S. collected and processed data; I.H.,
285 S.D., and T.P. performed the analyses; I.H. and U.J. wrote the paper.

A filament, hook, rods, MotB, MotA, MS-ring, Mot stator, H⁺, H⁺, switch

B z, x

C y, x

D Flow

schematic

Bright field

Holdfast

time (min)   -12   -8   -4   0

E Fraction of attached daughters (%)

wt   ΔpilA   ΔfliFG   ΔflgDE   ΔmotA   ΔfliL

F Flow, seeding cell, 6 mm

G Normalized microcolony area

wt   ΔpilA   ΔmotB   motB$_{D33N}$ ΔflgDE   ΔflgFG   ΔflgDE ΔmotB   ΔflgDE motB$_{D33N}$ ΔflgDE ΔpilA

H Time between cell separation and holdfast detection (min)

ΔflgDE   motB$_{D33N}$ ΔflgDE ΔpilA   ΔflgDE ΔcpaF   ΔflgDE motB$_{D33N}$ ΔflgDE ΔcpaE

A

rel. c-di-GMP binding

[³³P] c-di-GMP (µM)

rel. cdG binding

– cdG GMP GTP AMP

B

```
                                         R23    R27
C.c.   MFV--PQEQSGLNEAAP-----AAPRRPYRLSRRPEER | VHVLGGTMDLVRPEEVFHFV
C.h.   MFL--PA----RDATSP------EVRQNFRMNRRPEER | VQVLGGSMDLVRPEEVFHFV
C.sp.  MFL--PA----RDAFSP------EARQNFRLNRRPEER | VQVLGGSMDLVRPEEVFHFV
B.d.   MYHAPPG----FDPSGPPPDRRRRQRAPFRQSRRPDER | ITLLGEPVDLVRPEEVLLLL
B.n    MYYAPPG----FDPSGPPPDRRRRPRAPFRQTRRPDER | IALLGEPVDLVRPEEVLLHL
A.bi.  METPCR-------------------------------- | FSLLGAEVDTVTSAQMLDFA
A.be.  METPCR-------------------------------- | FSLLGAEVDRVTPACVMEFV
D.a.   MQQ----------------------------------- | IKVLGVSVNTMRISDLHSVI
R.m.   MR------------------------------------ | ISLLGVTVNAVTIEDLNLCI
L.t.   M------------------------------------- | POILGVSVDALTMDDLHRII
```

C

rel. c-di-GMP binding

WT R27A   cdG GTP ATP

WT R23A

HfsJ: WT   R23Q   R27A   R247Q

D

relative intensity of holdfast signal

HfsJ: WT   R23Q   R247Q

E

pili

flagellum

DgcB   rotor/stator   c-di-GMP

holdfast machinery (HfsJ)

holdfast

Isabelle Hug, Siddharth Deshpande, Kathrin S. Sprecher, Thomas Pfohl, Urs Jenal

correspondence to: urs.jenal@unibas.ch

This PDF file includes:

Materials and Methods
Figs. S1 to S7
Captions for Tables S1 to S4
Captions for Movies S1 to S6

Other Supplementary Materials for this manuscript includes the following:

Tables S1 to S4
Movies S1 to S6

Materials and Methods

Bacterial strains and growth conditions

Strains, plasmids and oligonucleotides used are described in Supplementary Information Tables S2-4. *C. crescentus* strains were grown in PYE medium at 30°C with agitation. Antibiotics (kanamycin, 5 μg/ml; chloramphenicol 1 μg/ml, tetracycline, 2.5 μg/ml) and inducers (Isopropyl β-D-1-thiogalactopyranoside (IPTG, Sigma), 100 μM or 500 μM; xylose, 0.3%) were added to the growth medium where required.

Microfluidics

Polydimethylsiloxane (PDMS) microfluidics devises were produced with photolithography as described elsewhere (*12*). Fresh medium was fed with a polytetrafluoroethylene (PTFE) microtube (0.56 x 1.07 mm, Fisher Scientific) from a 1 ml syringe (Soft-ject, Henke-Sass, Wolf), connected with a needle (0.6 x 30 mm, B-Braun Melsungen AG). Flow was driven by a pump (Type 871012, B-Braun Melsungen AG) adjusted to carry 1 ml syringes and applying flow rates of 0.002 μl/s in the flow channel (unless stated otherwise). The dimensions of the flow channel were 1 cm in length, 40 μm in width and 15 μm in height, and the channel was bordered by an inlet and an outlet. To avoid cells in the inlet, sterile PYE medium was first entered through the inlet until the start of the channel was filled. The bacterial culture was then introduced through the outlet, slowly approaching the front of the sterile medium which was kept in place while the air separating the two liquid phases escaped through the PDMS. Medium flux was initiated immediately after the two liquid phases merged. Microchamber devices were designed as rows of microchambers connected to one of two main channels between inlet and outlet of the same dimensions as described above. Chambers were squares of 40 μm and 0.75 μm in height.

Isolation of SW cells

For attachment-based synchronization, liquid cultures were grown in standard petri-dishes to mid-log phase. The medium containing non-attached cells was removed and the dishes were thoroughly washed with 30°C tap water. 1 ml fresh medium was added and freshly born SW cells were harvested after 5 min incubation at room temperature. Isolation of SW cells by Ludox density synchronization was described elsewhere (*27*).

Microscopy

Microscopy images were acquired with a Delta Vision Core microscope (GE Healthcare), equipped with a UPlan FL N 100x and a UPlanSApo 100x oil objective (Olympus) for phase contrast and bright field microscopy respectively and a pco.edge sCMOS camera. Images were acquired using softWoRx 6.0 software (GE Healthcare), and ImageJ 1.49e software was used to process and analyze images. Cells were either grown in microfluidics devices or spotted on agarose pads (Sigma, 1% in water) and kept at 30°C during microscopy. To avoid surface induced behavioral changes when cells were spotted on agarose pads, cells were inactivated by addition of carbonyl cyanide m-chlorophenyl hydrazine (CCCP, 200 μM) or formaldehyde (4%) for 15 min previous to analysis. For visualization of the holdfast, Oregon Green 488-, Texas Red-X- or Alexa Fluor 350-labelled WGA lectin was added to the culture (1 μg/ml, Invitrogen). CtrA-YFP,

expressed from the plasmid pEJ146 by addition of 0.3% xylose for induction, served as marker of the developmental stage of single cells. SW cells were identified by morphology (short, no stalk) and cytoplasmic florescence. DgcB localization was studied by expressing DgcB-venus from plasmid pSA232 by induction with IPTG (500 μM). The GFP filter-set was used for images with WGA-488 (peak wavelengths 470 nm for excitation and 525 nm for emission), the mCherry filter-set for WGA-Texas Red-X (572 nm excitation, 632 nm emission), the CFP filter-set for WGA-350 (430 nm excitation, 470 nm emission) and the YFP filter-set for DgcB-YFP and CtrA-YFP constructs (500 nm excitation, 535 nm emission).

For high speed movies, images were taken at a frame rate of 500 frames per second. To monitor holdfast appearance in microchambers, a frame rate of 4 frames per minute was chosen. This allowed the tracking of individual cells as they moved passively in the medium. Because of the high swimming speed of *C. crescentus* and its sensitivity to phototoxic effects, tracking was conducted with non-motile cells (Δ*flgDE*) and light intensities and exposure times were chosen at the lower limit, to provide sufficient image quality while avoiding phototoxic effects from excessive illumination.

Immunoprecipitation

For the identification of proteins located in proximity of each other, cells expressing His_{10}-tagged DgcB or MotA from their native chromosomal locus were harvested from 1 l cultures grown to mid-log phase. The pellets were resuspended in 5 ml phosphate buffer (39 mM Na_2HPO_4, 22 mM KH_2PO_4, 68 mM NaCl) and cross-linked by addition of 500 μl dithiobis(succinimidyl propionate) (DSP, ThermoFisher: 20 mM in dimethyl sulfoxide (DMSO, Sigma)) and incubation for 40 min at room temperature. Cross-linking was stopped with 611 μl 1 M Tris-HCl, pH 8. After further incubation for 30 min, the samples were stored at -80°C until further processing. Proteinase inhibitor cocktail (1/4 of a tablet, cOmplete Mini, Roche) was added to the cross-linked cell suspension which was then lysed by french press (mini cell, 15000 PSI, Thermo Scientific). The lysate was mixed 1:1 with 2x loading buffer (16 M urea, 600 mM NaCl, 1% SDS, 0.5% n-Dodecyl β-D-maltoside (DDM), pH 8.0) and solubilized overnight at room temperature while rotating. Particles and insoluble debris was removed by centrifugation for 30 min at 4000 g and room temperature. The supernatant was loaded on 50 μl Ni-NTI agarose beads (Machery-Nagel) overnight with rotation. The beads were washed twice each with 1 ml wash buffer 1 (10 mM Tris-HCl pH 6.8, 200 mM NaCl, 8 M urea, 0.5% SDS) and wash buffer 2 (20 mM Tris-HCl pH 8.0, 250 mM NaCl, 4 M urea, 0.5% SDS, 5 mM imidazole), and purified proteins were eluted with 50 μl elution buffer (50 mM Tris-HCl pH 6.8, 400 mM Imidazole, 200 mM NaCl, 4 M urea, 0.5% SDS). Proteins were separated by SDS-PAGE as described below. Entire gel-columns corresponding to one sample were cut, trypsin digested and subjected to MS analysis.

Immunoblots

Harvested cell pellets were resuspended in 100 μl per OD660 of sample buffer (0.1 M Tris pH 6.8, 5% Glycerol, 0.2 % sodium dodecyl sulfate (SDS), 1 % β-Mercaptoethanol, 0.025 % Bromophenol blue) and cooked for 5 min at 95° C. Proteins were separated by electrophoresis on 12% SDS-polyacrylamide gels and transferred onto polyvinylidene fluoride (PVDF)-membranes (Immobilon-P, Millipore, USA). PageRuler Prestained

Protein Ladder (ThermoFisher) served to mark protein sizes. Primary antibodies used for detection were polyclonal rabbit anti-DgcB (Josman LLC, USA) and monoclonal mouse anti-Flag M2 (Sigma), and secondary antibodies were swine anti-rabbit and rabbit anti-mouse, respectively, coupled to horseradish peroxidase (Dako, Denmark). Dilutions of 1:10000 were used for all antibodies. Antibody-treated blots were incubated with LumiGLO (KPL) for exposure of super RX-N films (Fujifilm).

In silico analysis
Proteins related to DgcB were identified by an iterative search against the rp55 database using Jackhmmer (www.ebi.ac.uk/Tools/hmmer/search/jackhmmer) with full length DgcB sequence as query. Hits without a GGDEF domain were removed manually. To find highly conserved residues in the N-terminus, the search was repeated using the first 100 residues of the DgcB sequence as query. Proteins containing the motif [LMI]-x-x-x-x-[LIVM]-x-[PAVFM]-[TSIYH]-[PA]-x-[NAH]-[YF]-x-x-[WAVLIFYQ]-[YFH]-x-x-x-x-x-x-x-x-[LAVFM], derived from the conservation profile of the DgcB N-terminus (see Fig. S6c), were identified using MOTIF Search (www.genome.jp/tools/motif/MOTIF2.html). To identify arginines specific for the HfsJ variants of species closely related to *C. crescentus* which may play a role in c-di-GMP binding, a protein Blast search was performed using the blast.ncbi.nlm.nih.gov website, and the sequences of selected hits were aligned using the T-Coffee software on the tcoffee.crg.cat website.

HfsJ over-expression and UV-cross linking
One liter of LB medium substituted with chloramphenicol (20 μg/ml), kanamycin (30 μg/ml) and IPTG (0.5 mM) was inoculated with 1 ml overnight culture of *E. coli* Rosetta strains carrying the *hfsJ-his$_8$* gene variants on pET42b. Cultures were grown at 30°C with 200 rpm agitation and harvested in exponential growth phase. Cell pellets were stored at -80°C until further processing. Cells were resuspended in 2 ml TBS buffer (20 mM Tris-HCl pH 7.5, 150 mM NaCl, 2.5 mM KCl) substituted with proteinase inhibitor cocktail (1/10 of a tablet, cOmplete Mini, Roche) and were lysed using a mini French press cell (15000 PSI, Thermo Scientific). Protein content of the lysates was determined with a Nanodrop device (Titertek-Berthold) and concentrations of 20 mg/ml protein were adjusted by addition of TBS.
[^{33}P]c-di-GMP synthesis was performed as described elsewhere (*28*). 16 mg protein solutions were mixed with the appropriate concentration of [^{33}P]c-di-GMP and adjusted with TBS buffer to a final volume of 30 μl. For nucleotide competition, binding of 5 μM [^{33}P]c-di-GMP was competed with 500 μM cold c-di-GMP, GMP, GTP or AMP (Sigma). After 10 min incubation at room temperature, the samples were exposed to irradiation for 3 min at 254 nm and 4°C for crosslinking. After diluting into sample buffer, the proteins were separated by SDS-PAGE as described above. The gels were dried before exposure of a phosphor screen. Protein bands containing [^{33}P]c-di-GMP were detected by scanning the phosphor screens with a Typhoon FLA 7000 imaging system (GE Healthcare) and band intensities were quantified using ImageJ 1.49e software. Binding curves were fitted with GraphPad Prism 6.0.
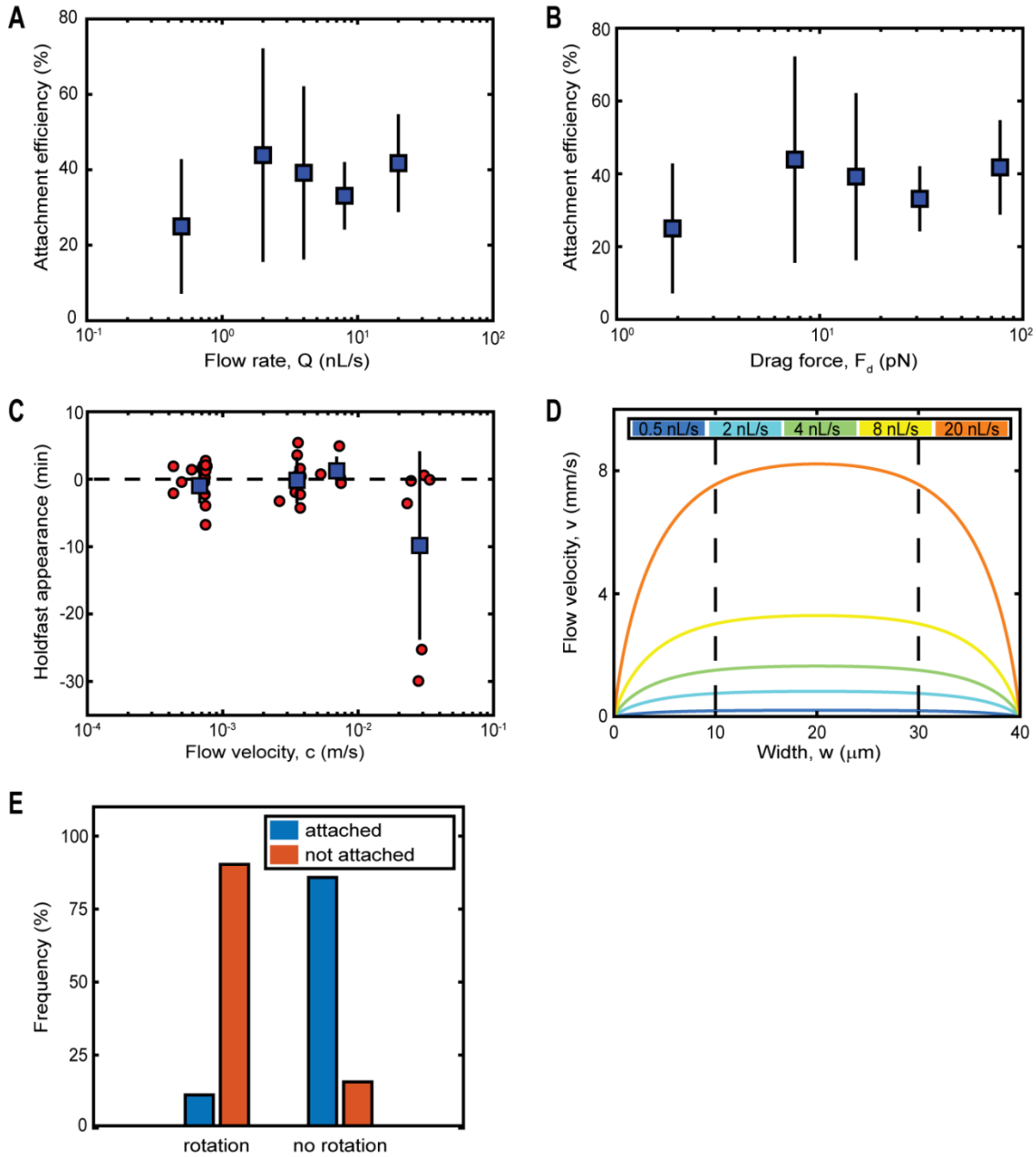
Fig. S1. Flow-induced surface contact stimulates *C. crescentus* surface attachment. Attachment efficiency of daughter cells in microchannels, plotted for different flow rates (**A**) and the corresponding drag forces (F_d) (**B**). Cells were approximated as spheres with a radius $r = 0.5$ μm. F_d was calculated as $6\pi\eta r\upsilon$, where η is the fluid viscosity ($\approx 10^{-3}$ Pas), and υ is the maximum fluid velocity at a distance of 0.5 μm from the channel wall. Number of cells analyzed: 38 (0.5 nl/s), 21 (2 nl/s), 24 (4 nl/s), 39 (8 nl/s), and 54 (20 nl/s). (**C**) Time of holdfast appearance with respect to the separation of SW cells from their mothers (0 min) plotted for different flow velocities. Squares represent sample

means and error bars indicate standard deviations. The scatter represents the flow velocity depending on the position of the cell in the microchannel. (**D**) Flow velocity profile along the width of the channel, for different flow rates (*29*). The vertical dashed lines indicate the middle 50% area of the microchannel; only cells attached within this area were used for calculating the attachment efficiency in (**A**) and (**B**). (**E**) Fate of SW cells in microchannels that either rotated or were paralyzed immediately before separation from their mothers. The fraction of cells that were released or adhered downstream of their mothers is indicated.
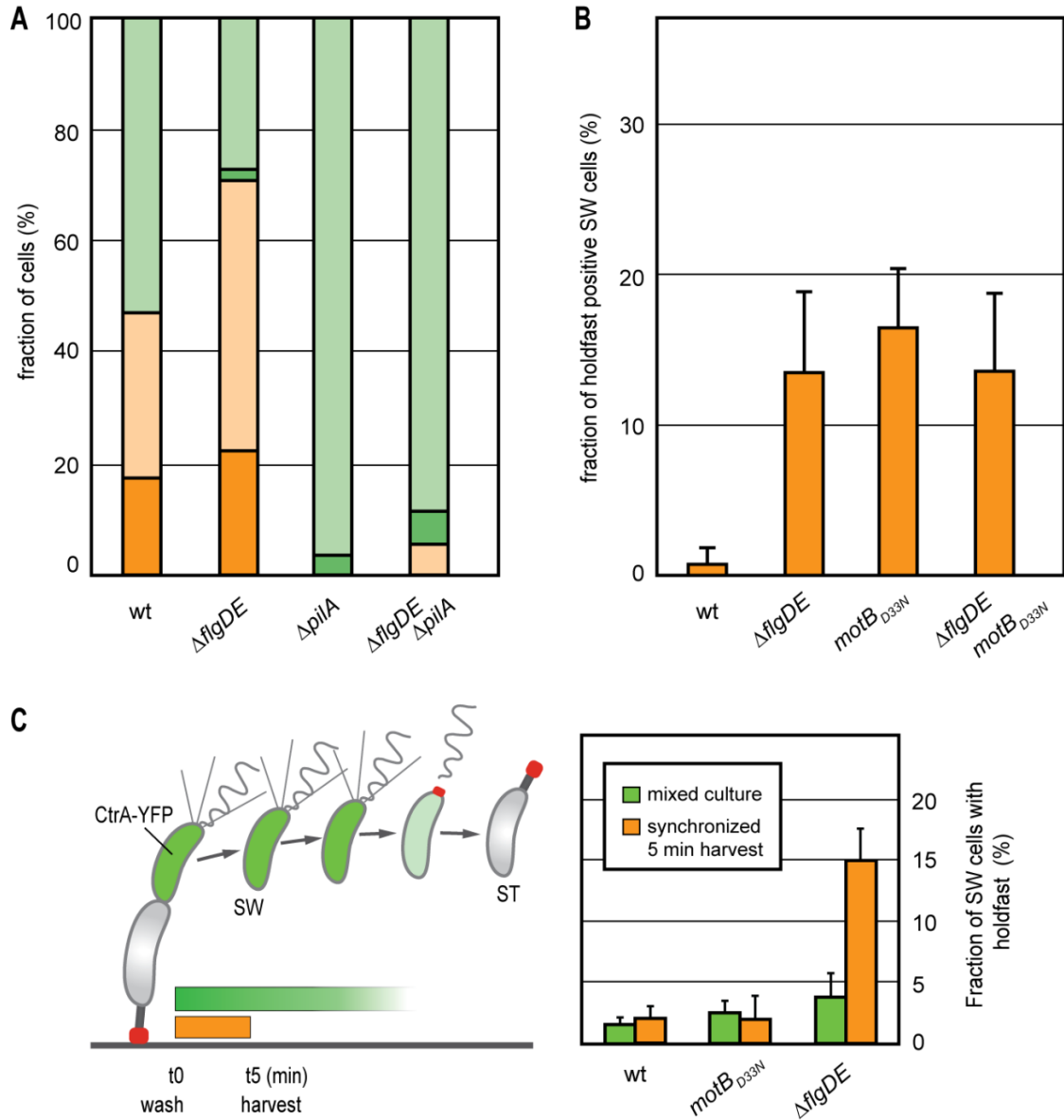
Fig. S2. Mutants lacking hook and filament do not produce premature holdfast.
(**A**) The fraction of SW cells exposing a holdfast before separation from their mother was not increased in the *ΔflgDE* mutant. SW cells that remained attached (orange) or were washed away (green) after separating from their mother in microchannels were scored. Dark and light colors represent fraction of cells with and without a holdfast formed before cell division, respectively. Of the attaching cells 37.5% (wt) and 35.3% (*ΔflgDE*) displayed holdfast already before division. n= 17 (wt), 48 (*ΔflgDE*), 28 (*ΔpilA*) and 17 (*ΔflgDE ΔpilA*). (**B**) SW cells were isolated by Ludox density gradient centrifugation and were scored for the presence of a holdfast using fluorescently labeled WGA. Non-motile mutant strains showed a modest increase of holdfast positive cells. This is explained by the delayed separation of paralyzed daughters from their mothers and the resulting advance of the developmental program upon birth. Importantly, the *ΔflgDE* and *motB*$_{D33N}$

mutants showed similar numbers of holdfast positive cells. n= 2720 (wt), 1358 (*ΔflgDE*), 1569 (*motB$_{D33N}$*) and 1291 (*ΔflgDE motB$_{D33N}$*). Bars represent averages of individual microscopy images and error bars represent standard deviations. (**C**) To avoid synchronization techniques and thus minimize the probability of cells experiencing surface contact during experimental handling (e.g. centrifugation) holdfast was scored in strains expressing CtrA-YFP (green), a SW stage-specific fusion protein that allows identifying newborn cells microscopically (*30*). SW cells from the same liquid cultures were isolated before (green) and after (orange) synchronization using an attachment-based synchronization technique (*31*).While *ΔflgDE* mutant cells that did not experience experimental synchronization showed wild type-like fractions of holdfast positive cells, the fraction of holdfast-bearing cells was increased in *ΔflgDE* (but not *motB$_{D33N}$*) mutant cells upon mild surface exposure during synchronization. n= 1460 (wt, mixed culture), 2219 (wt, synchronized), 1600 (*motB$_{D33N}$*, mixed culture), 369 (*motB$_{D33N}$*, synchronized); 1065 (*ΔflgDE*, mixed culture), 335 (*ΔflgDE*, synchronized). Bars represent the average of two independent experiments and error bars show standard deviations.
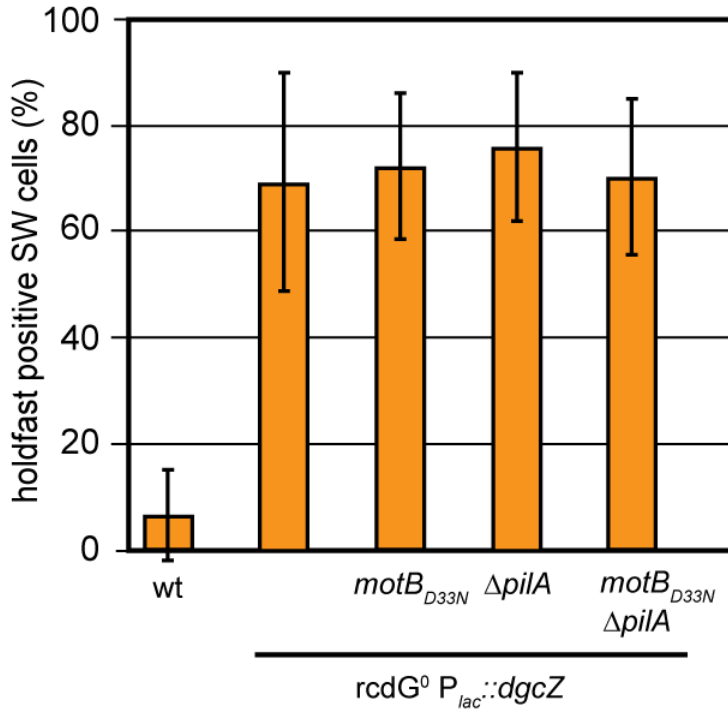
Fig. S3. C-di-GMP bypasses the requirement for an active motor and pili to induce holdfast production.

Holdfast expression of SW cells grown with minimal surface contact in liquid culture (see Fig. S2C, without synchronization) was scored. *dgcZ* expression was induced with 100 µM IPTG. Data are based on 347 (wt), 166 (rcdG^0 P$_{lac}$::*dgcZ*), 277 (rcdG^0 P$_{lac}$::*dgcZ motB$_{D33N}$*), 287 (rcdG^0 P$_{lac}$::*dgcZ ΔpilA*) and 296 (rcdG^0 P$_{lac}$::*dgcZ motB$_{D33N}$ ΔpilA*) individual SW cells. Bars show averages and error bars show the standard deviations of the data obtained from individual microscopy images.
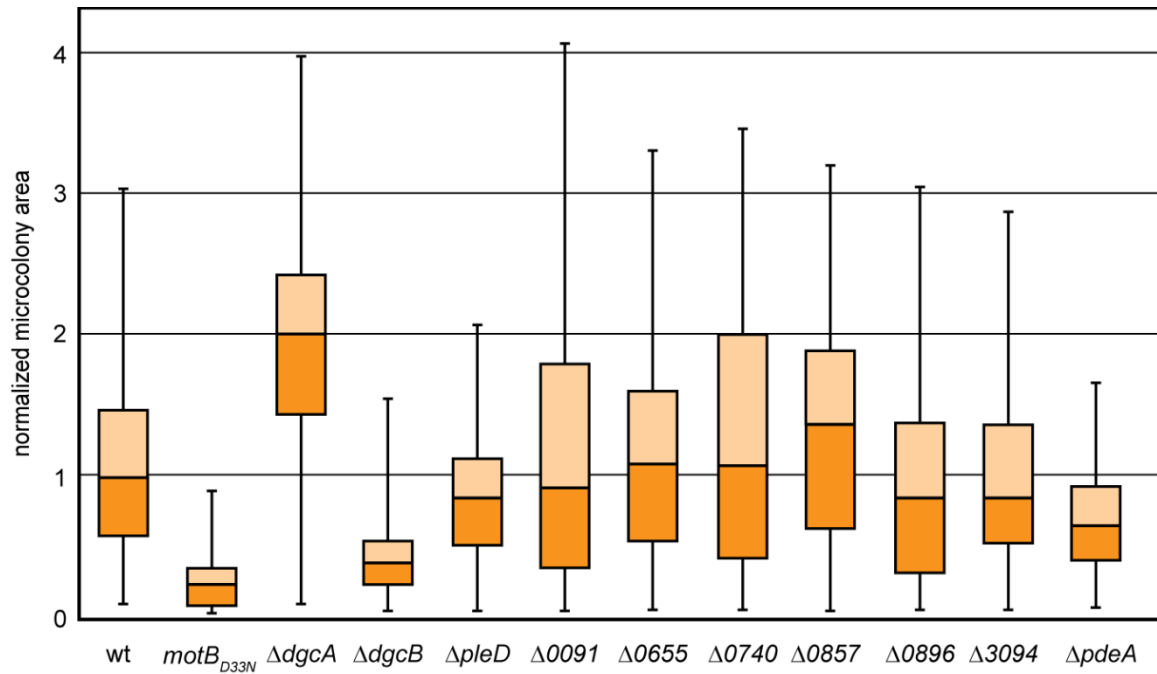
Fig. S4. The DgcB diguanylate cyclase is essential for rapid surface response.
Strains with individual deletions in genes encoding *C. crescentus* diguanylate cyclases or the principal phosphodiesterase PdeA, were analyzed for rapid attachment under flow. The surface-blind *motB*$_{D33N}$ mutant is shown as control. Box plots show the median (horizontal black lines), the lower and upper quartiles (dark and light orange boxes) and the extreme values (whiskers). The median of the wild type (relative value 1) corresponds to 129.8 μm^2.

A
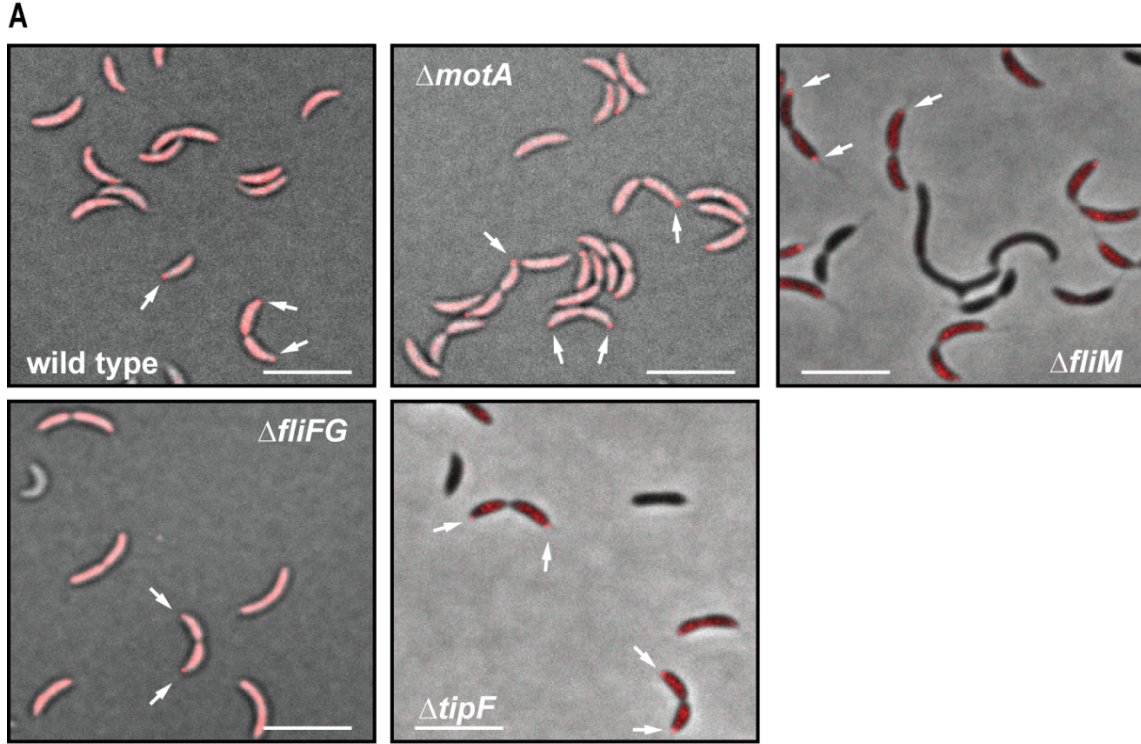
B

Strain	Score	Coverage	Peptide identified
wt	-	-	-
His10-DgcB	35.14	8.33	GNVPSAYQPSFAELEEALSQmPNE
DgcB-His10	23.29	8.33	GNVPSAYQPSFAELEEALSQmPNE
	27.26	3.82	DLLSLLFLLTK
MotB-His10	46.74	3.68	DATTDGLTNLANR

Fig. S5. DgcB co-localizes with the flagellar motor.
(**A**) DgcB-YFP was expressed from a plasmid to determine its localization behavior. The cyclase localized to the flagellated pole in late pre-divisional and SW cells (arrows) as expected for a protein orchestrating the tactile response. Localization was not disturbed in strains with a paralyzed flagellum (*ΔmotA*) or lacking different parts of the flagellum (*ΔfliM*, *ΔfliFG*, *ΔtipF*). White scale bars represent 5 μm. (**B**) Identification of peptides from pulldown experiments corroborate the close proximity of DgcB and MotA. Mass spectrometry of pull-down eluates of His10-tagged DgcB or MotA identified peptides of the respective other protein. No peptides of DgcB or MotA were found in pull-downs with a wild-type control.
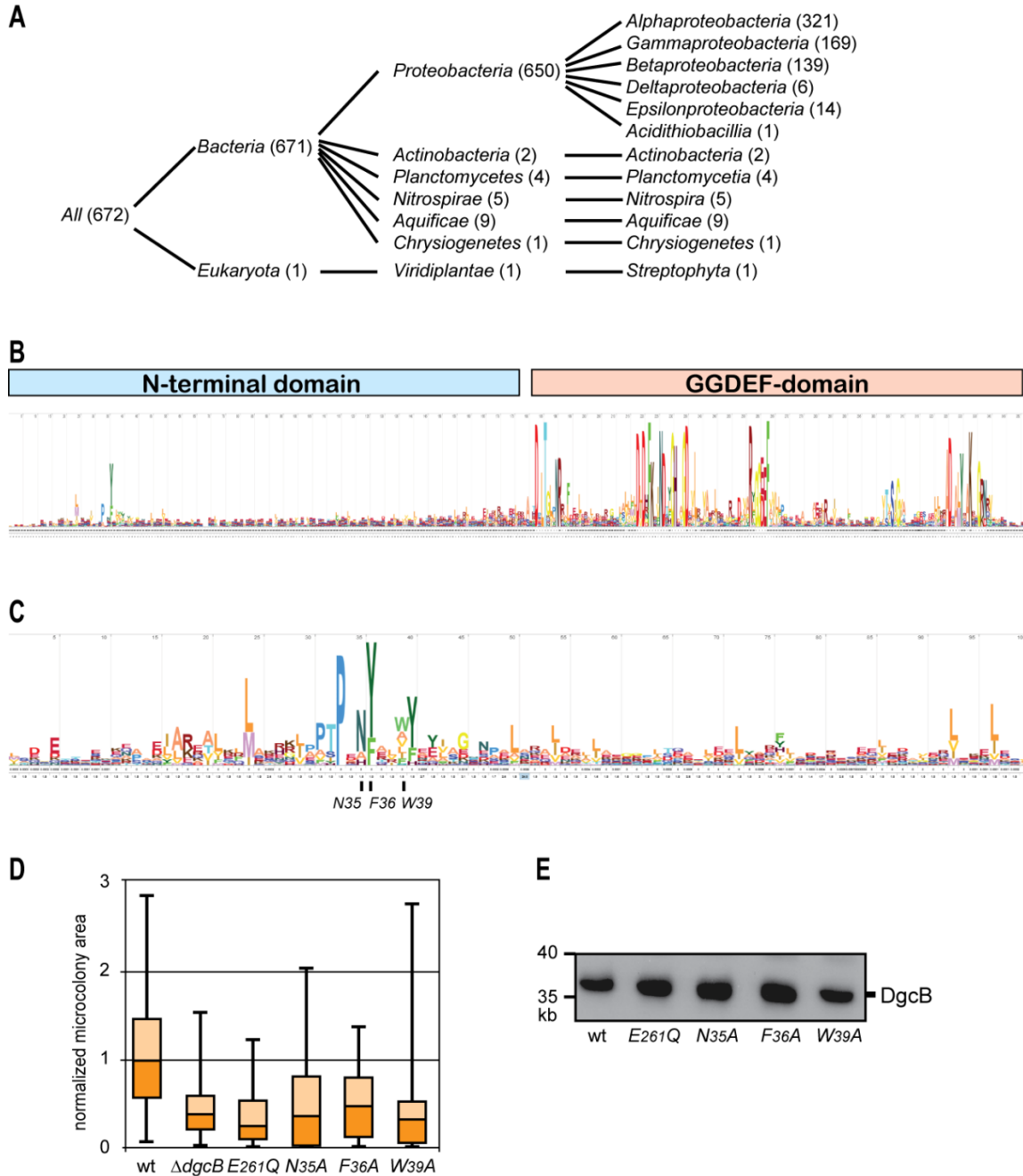
11

Fig. S6. The N-terminus of DgcB is a putative signal input domain.
(**A**) Prevalence of DgcB orthologues. Jackhmmer analysis against the rp55 database was carried out with the full length DgcB sequence as query. All hits lacking a GGDEF domain were excluded. Shown are results obtained in the second iteration. (**B**) Weblogo illustration of amino acid conservation of DgcB orthologues. The N-terminal (blue) and the GGDEF (red) domains are outlined. (**C**) Analysis of amino acid conservation in the N-terminal domain of DgcB. Jackhmmer analysis against the rp55 database using amino acid residues 1-100 as query. Shown are results obtained in the fifth iteration. The three highly conserved residues that were analyzed experimentally (N35, F36, W39) are

marked. (**D**) Rapid attachment efficiency in flow chambers of *dgcB* alleles harboring point mutations in conserved residues of the N-terminal domain. Controls include the *ΔdgcB* strain and a strain expressing a catalytic mutant of DgcB (*dgcB$_{E261Q}$*). Box plots show the median (horizontal black lines), the lower and upper quartiles (dark and light orange boxes) and the extreme values (whiskers). The median of the wild type (relative value 1) corresponds to 129.8 μm^2. (**E**) Immunoblot analysis of the cellular concentrations of DgcB wild-type and mutant variants using an anti-DgcB antibody.
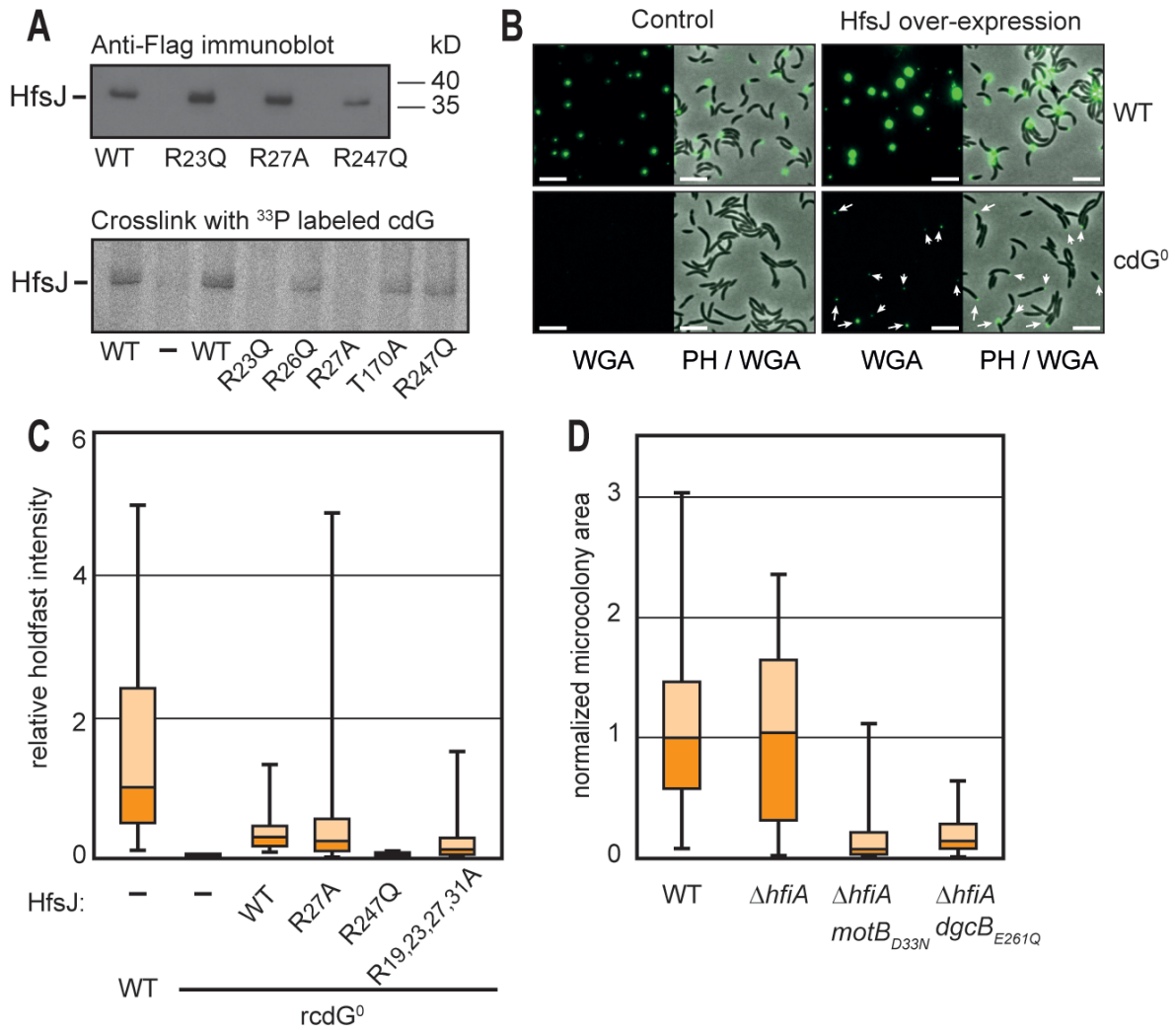
Fig. S7. The HfsJ glycosyltransferase is a c-di-GMP effector.
(**A**) Top: Immunoblot of strains carrying Flag-tagged *hfsJ* alleles using an anti-Flag antibody. Bottom: c-di-GMP binding to HfsJ variants using a UV-crosslink assay with ^{33}P labeled c-di-GMP. (**B**) Microscopy analysis of holdfast expression using fluorescent WGA. Strains in panels on the left contain a control plasmid, strains in panels on the right harbor a plasmid overexpressing *hfsJ*. Panels show fluorescence (WGA) or an overlay of fluorescence and phase contrast (PH). Arrows mark holdfast structures in the cdG^0 strain overexpressing *hfsJ*. White scale bars represent 5μm. (**C**) Quantification of holdfast using fluorescent WGA of cells over-expressing wild-type or mutant HfsJ variants from a plasmid. Numbers of cells analyzed: 43 (wt, empty vector), 2 (rcdG^0, empty vector), 44 (rcdG^0, wt), 307 (rcdG^0, R27A), 5 (rcdG^0, R247Q), 321 (rcdG^0, R19,23,27,31A). (**D**) Rapid surface attachment of SW cells is not dependent on HfiA. Wild-type and mutant strains were used as indicated. Box plots in (**C**) and (**D**) show the median (horizontal black lines), the lower and upper quartiles (dark and light orange boxes) and the extreme values (whiskers). Values are normalized to the median of the wild-types.

Table S1.

List of proteins containing the motif [LMI]-x-x-x-x-[LIVM]-x-[PAVFM]-[TSIYH]-[PA]-x-[NAH]-[YF]-x-x-[WAVLIFYQ]-[YFH]-x-x-x-x-x-x-x-x-x-[LAVFM] found in the N-terminal domain of DgcB.
Excel sheet 1.

Table S2.

Strains used in this work.
Excel sheet 2.

Table S3.

Plasmids used in this work.
Excel sheet 3.

Table S4.

Oligonucleotides used in this work.
Excel sheet 4.

Movie S1

C. crescentus cell division in a microfluidic flow channel. Holdfast is visualized using fluorescent WGA lectin. Note that in this representative example, a holdfast structure is visible at the flagellated pole of the SW progeny before separation from its mother cell.

Movie S2

High speed imaging of a representative SW cell that fails to attach to the surface after separating from its mother in a microfluidic flow channel. Note that SW cells that initiate rotation before separating from their mother generally do not attach.

Movie S3

High speed imaging of a representative SW cell that attaches to the surface after separating from its mother in a microfluidic flow channel. Note that SW cells that remain paralyzed before separating from their mother generally attach immediately downstream of their mother.

Movie S4

High speed imaging of a representative SW cell that attaches to the surface after separating from its mother in a microfluidic flow channel. Note that this SW cell stops rotation before separating from its mother and remains surface attached.

Movie S5

Cycles of growth and division in a microfluidic flow channel result in the formation of microcolonies from single founder cells.

Movie S6

Time lapse of a dividing *C. crescentus* cell grown in a microfluidic flow channel that expressed a DgcB-Venus fusion. Note that DgcB localizes to the flagellated cell pole before and after cell division.